Neurobiology of Disease

Aberrant Sodium Channel Currents and Hyperexcitability of Medial Entorhinal Cortex Neurons in a Mouse Model of *SCN8A* Encephalopathy

Matteo Ottolini,[1]* Bryan S. Barker,[1,2]* Ronald P. Gaykema,[1] Miriam H. Meisler,[3] and Manoj K. Patel[1,2]

[1]Department of Anesthesiology and [2]Neuroscience Graduate Program, University of Virginia Health System, Charlottesville, Virginia 22908, and [3]Department of Human Genetics, University of Michigan, Ann Arbor, Michigan 48109

SCN8A encephalopathy, or early infantile epileptic encephalopathy 13 (EIEE13), is caused predominantly by *de novo* gain-of-function mutations in the voltage-gated Na channel $Na_v1.6$. Affected individuals suffer from refractory seizures, developmental delay, cognitive disability, and elevated risk of sudden unexpected death in epilepsy (SUDEP). A knock-in mouse model carrying the patient mutation p.Asn1768Asp (N1768D) reproduces many features of the disorder, including spontaneous seizures and SUDEP. We used the mouse model to examine the effects of the mutation on layer II stellate neurons of the medial entorhinal cortex (mEC), which transmit excitatory input to the hippocampus. Heterozygous ($Scn8a^{D/+}$), homozygous ($Scn8a^{D/D}$), and WT ($Scn8a^{+/+}$) littermates were compared at 3 weeks of age, the time of seizure onset for homozygous mice. Heterozygotes remain seizure free for another month. mEC layer II neurons of heterozygous and homozygous mice were hyperexcitable and generated long-lasting depolarizing potentials with bursts of action potentials after synaptic stimulation. Recording of Na currents revealed proexcitatory increases in persistent and resurgent currents and rightward shifts in inactivation parameters, leading to significant increases in the magnitude of window currents. The proexcitatory changes were more pronounced in homozygous mice than in heterozygotes, consistent with the earlier age of seizure onset in homozygotes. These studies demonstrate that the N1768D mutation increases the excitability of mEC layer II neurons by increasing persistent and resurgent Na currents and disrupting channel inactivation. The aberrant activities of mEC layer II neurons would provide excessive excitatory input to the hippocampus and contribute to hyperexcitability of hippocampal neurons in this model of *SCN8A* encephalopathy.

Key words: action potential; entorhinal cortex; epilepsy; epileptic encephalopathy; SCN8A; sodium channels

Significance Statement

SCN8A encephalopathy is a devastating neurological disorder that results from *de novo* mutations in the Na channel $Na_v1.6$. In addition to seizures, patients suffer from cognitive and developmental delays and are at high risk for sudden unexpected death in epilepsy (SUDEP). A mouse knock-in model expressing the patient mutation N1768D reproduces several pathological phenotypes, including spontaneous seizures and sudden death. We demonstrate that medial entorhinal cortex (mEC) neurons from the mouse model exhibit proexcitatory alterations in Na channel activity, some of which were not seen in hippocampal or cortical neurons, and resulting in neuronal hyperexcitability. Because mEC neurons regulate the activity of the hippocampus, which plays an important role in seizure onset, we propose that these profound changes in mEC neuron excitability associated with the gain-of-function mutation of $Na_v1.6$ may increase excitatory drive into the hippocampus, culminating in seizure activity and SUDEP.

Introduction

The voltage-gated Na channel $Na_v1.6$ plays a major role in neuronal excitability (Lorincz and Nusser, 2008; Vacher et al., 2008; Hu et al., 2009). $Na_v1.6$ is concentrated at the axon initial segment (AIS), the site of initiation of action potentials (APs), and at the nodes of Ranvier, responsible for saltatory conduction (Boiko et al., 2001; Kaplan et al., 2001; Hu et al., 2009; Rasband, 2010). $Na_v1.6$ contributes to spike threshold and repetitive firing in neu-

Received Aug. 26, 2016; revised June 6, 2017; accepted June 27, 2017.

Author contributions: M.O., B.S.B., R.P.G., M.H.M., and M.K.P. designed research; M.O., B.S.B., and R.P.G. performed research; R.P.G. and M.H.M. contributed unpublished reagents/analytic tools; M.O., B.S.B., and M.K.P. analyzed data; M.O., B.S.B., M.H.M., and M.K.P. wrote the paper.

This work was supported by National Institute for Neurological Disorders and Stroke–National Institutes of Health Grant R01NS075157 to M.K.P. and Grant RO1NS34509 to M.H.M.).

The authors declare no competing financial interests.

*M.O. and B.S.B. contributed equally to this work.

Correspondence should be addressed to Manoj K. Patel, Ph.D., Department of Anesthesiology, University of Virginia Health System, 1 Hospital Drive, Box 800710, Charlottesville, VA 22908-0710. E-mail: mkp5u@virginia.edu.

DOI:10.1523/JNEUROSCI.2709-16.2017

 0270-6474/17/377643-13$15.00/0

rons (Raman et al., 1997; Levin et al., 2006; Royeck et al., 2008; Hargus et al., 2011). The endogenous properties and expression patterns of $Na_v1.6$ make this channel a prime candidate for facilitating the neuronal hyperexcitability that is associated with epilepsy. Proexcitatory alterations in Na channel activity contribute to seizure initiation and propagation in human patients (Vreugdenhil et al., 2004) and animal models of epilepsy (Kearney et al., 2001; Blumenfeld et al., 2009; Hargus et al., 2011, 2013; Lopez-Santiago et al., 2017), whereas decreased $Na_v1.6$ activity reduces the development of seizures (Martin et al., 2007; Blumenfeld et al., 2009).

De novo mutations of *SCN8A*, encoding $Na_v1.6$, are responsible for early infantile epileptic encephalopathy 13 (EIEE13), also referred to as *SCN8A* encephalopathy (OMIM #614558) (Wagnon and Meisler, 2015; Meisler et al., 2016). To date, >100 *de novo* mutations of *SCN8A* have been identified. Nine of the 11 mutations that have been electrophysiologically evaluated display gain-of-function features, including impaired inactivation and premature channel opening (Wagnon and Meisler, 2015; Wagnon et al., 2016; Barker et al., 2016). Patients with EIEE13 experience seizure onset between birth and 18 months of age and *in utero* seizures have been reported (Singh et al., 2015). Patients also suffer from mild to severe intellectual disability and movement disorders (Hammer et al., 2016). SUDEP has been reported in 10% of EIEE13 patients (Veeramah et al., 2012; Kong et al., 2015; Larsen et al., 2015; Wagnon and Meisler, 2015).

The first described *SCN8A* encephalopathy mutation, p.Asn1768Asp (N1768D), was identified in a child who had onset of refractory epilepsy at 6 months of age, intellectual disability, ataxia, and SUDEP at 15 years (Veeramah et al., 2012). Studies of the mutant channel in transfected cells revealed gain-of-function characteristics including increased persistent Na currents, disruptions in channel inactivation, and increased resurgent current (Veeramah et al., 2012; Patel et al., 2016). Expression of the mutant channel in cultured hippocampal neurons resulted in elevated rates of spontaneous firing (Veeramah et al., 2012). A knock-in mouse carrying the N1768D mutation (Jones and Meisler, 2014) exhibits many pathological phenotypes seen in the patient, including spontaneous seizures and sudden death (Wagnon et al., 2015). In homozygous mutant mice, seizures begin at 3 weeks of age and progress to death within 24 h of onset. In heterozygous mutant mice, seizures begin between 2 and 4 months of age and progress to death within days (Wagnon et al., 2015). Due to incomplete penetrance, ~50% of heterozygous mice remain seizure free. Electrophysiological studies of CA1, CA3, and cortex layer 2/3 neurons of heterozygous mice revealed region-specific increases in persistent sodium current (I_{NaP}) in excitatory and inhibitory neurons, with CA1 pyramidal neurons being most affected (Lopez-Santiago et al., 2017). Although spike frequencies were not increased, CA1 neurons did exhibit early after depolarization-like events and there was spontaneous firing of CA1 and CA3 neurons that was not seen in the WT controls. Interestingly, Na channel activation and inactivation gating parameters were not altered in any of the neurons tested.

In the present study, we evaluated the effects of the $Na_v1.6$-N1768D mutation in layer II stellate neurons of the medial entorhinal cortex (mEC) and extended the studies to include both heterozygous and homozygous mutant mice. mEC layer II stellate neurons provide excitatory input to the dentate gyrus and CA3 neurons and elevate circuit excitability in animal models of temporal lobe epilepsy (Kobayashi et al., 2003; Hargus et al., 2011). We observed increased rates of AP firing and proexcitatory changes in Na channel properties of mEC neurons, with larger effects in homozygous mice than in heterozygotes. Changes were observed in neurons from heterozygous mice >1 month before seizure onset. These studies provide insight into the mechanisms by which a gain-of-function mutation in $Na_v1.6$ leads to increased neuronal excitability. Our studies provide support for the region specificity of alterations and suggest that the profound proexcitatory changes observed in mEC neurons increase network drive into the hippocampus, contributing to the development of spontaneous recurrent seizures.

Materials and Methods

Animals. *Scn8a*^{N1768D} knock-in mice were generated as described previously (Jones and Meisler, 2014; Wagnon et al., 2015). All animal experiments were conducted in accordance with the guidelines established by the National Institutes of Health's *Guide for the Care and Use of Laboratory Animals* and were approved by the University of Virginia's Institute of Animal Care and Use Committee. The line was maintained by backcrossing to C57BL/6J WT mice (The Jackson Laboratory catalog #JAX: 000664, RRID:IMSR_JAX:000664). Experiments were performed on male and female homozygous D/D mice (Scn8a$^{N1768D/N1768D}$), heterozygous D/+ mice (Scn8a$^{N1768D/+}$), and WT +/+ littermates at 3 weeks of age. The genotyping assay (Wagnon et al., 2015) was performed as follows. DNA was isolated from tail biopsies by digestion with 1 mg/ml proteinase K in buffer containing 50 mM KCl, 10 mM Tris-HCl, pH 8.0, and 0.1% Triton X-100. Genotyping used the introduced HincII site in the mutant allele (Jones and Meisler, 2014). A 327 bp genomic fragment of *Scn8a* containing the mutation was amplified by PCR with the primers Tar-F (5′-TGACT GCAGC TTGGA CAAGG AGC-3′) and Tar-R (5′-TCGAT GGTGT TGGGC TTGGG TAC-3′). PCR products were digested with HincII and analyzed on 2% agarose gels stained with ethidium bromide. The WT allele generates a single fragment of 327 bp and the mutant allele generates two fragments of 209 and 118 bp.

Brain slice preparation and AP recordings. Horizontal brain slices (300 μm) were prepared from D/D, D/+, and WT (+/+) mice. Mice were anesthesized with isoflurane, decapitated, and brains rapidly removed and placed in chilled (4°C) artificial CSF (ACSF) containing the following (in mM): 125 NaCl, 2.5 KCl, 1.25 NaH_2PO_4, 2 $CaCl_2$, 1 $MgCl_2$, 0.5 L-ascorbic acid, 10 glucose, 25 $NaHCO_3$, and 2 pyruvate oxygenated with 95% O_2 and 5% CO_2. Slices were prepared using a Vibratome 1000 Plus (Vibratome), transferred to a chamber containing oxygenated ACSF, incubated at 37°C for 35 min, and then stored at room temperature. For recordings, slices were held in a small chamber superfused with heated (32°C) oxygenated ACSF. mEC layer II neurons were visually identified by infrared video microscopy (Hamamatsu) using a Zeiss Axioscope microscope. Whole-cell voltage and current-clamp recordings were performed using an Axopatch 700B amplifier (Molecular Devices, pCLAMP 10 software) and a Digidata 1322A (Molecular Devices). Electrodes were fabricated from borosilicate glass using a Brown-Flaming puller (Model P97; Sutter Instruments) and had resistances of 3.5–4.0 MΩ when filled with an intracellular recording solution containing the following (in mM): 120 K-gluconate, 10 NaCl, 2 $MgCl_2$, 0.5 K_2EGTA, 10 HEPES, 4 Na_2ATP, 0.3 NaGTP, pH adjusted to 7.2 with KOH. Currents were amplified, low-pass filtered (2 kHz) and sampled at 33 kHz. APs were evoked with a series of current injection steps from −20 pA to 470 pA in 10 pA steps for 300 ms at 5 s interpulse intervals. In some experiments, a brief, 4 ms depolarizing current pulse was used to evoke APs. To standardize our tests, the resting membrane potential (RMP) was recorded and then maintained at −65 mV by injection of DC current. Cell input resistance (R_i) was calculated by dividing the steady-state voltage response evoked by varying current injections ($\Delta V/\Delta I$) from −20 pA until the current pulse just before that which evoked an AP. Data points were then fit with a linear line to determine R_i values. Threshold was determined as the voltage at which the slope of the AP exceeded ≥20 V/s. AP amplitudes were measured from threshold to the AP peak. AP duration (APD) was measured from threshold to the point at which the AP returned to the same potential. APD_{50} and APD_{90} were determined from this duration. Upstroke velocity was determined from phase plots using the maximum of the first derivative (dV/dt). In some experiments, APs

were evoked using a bipolar platinum iridium stimulating electrode (WPI) placed in layer III of the mEC ~1 mm distant from the mEC layer II neurons. A 400 μs stimulus of varying current amplitude (1 to 3.2 mA) was applied every 15 s via a digital stimulator (Digitimer). To evoke APs consistently, the stimulus amplitude was increased until there were no failures in spike initiation (1T). Duration of the evoked somatic response evoked by either electrical stimulation or via short depolarizing current pulses was determined as the interval between the start of the deviation from the RMP to the point at which the response returned to the RMP.

Na channel electrophysiology. All Na channel current recordings, except for persistent Na current (I_{NaP}) and resurgent Na current (I_{NaR}), were recorded using the outside-out recording configuration of the patch-clamp recording technique. Currents were amplified, low-pass filtered (2 kHz), and sampled at 33 kHz. Glass pipettes had resistance of 1.8–2.5 mΩ when filled with the following electrode solution (in mM): 140 CsF, 2 $MgCl_2$, 1 EGTA, 10 HEPES, 4 Na_2ATP, and 0.3 NaGTP, pH adjusted to 7.3 with CsOH, osmolarity adjusted to 310 MΩ with sucrose. Outside-out patches were superfused with solution containing the following (in mM): 150 NaCl, 2.5 KCl, 2 $CaCl_2$, 1 $MgCl_2$, 1.25 NaH_2PO_4, 0.5 L-ascorbic acid, 2 pyruvate, 10 glucose, 25 $NaHCO_3$, pH adjusted by bubbling 95% O_2 and 5% CO_2, osmolarity adjusted to 320 MΩ with sucrose. All experiments were performed at 32°C. Capacitive and leak currents were subtracted using the P/N-4 protocol. The current–voltage (*I–V*) relationship was determined using a 100 ms voltage pulse from −80 to +40 mV in steps of 5 mV from a holding potential of −120 mV at 2 s intervals. Conductance as a function of voltage was derived from the *I–V* relationship and fitted by a Boltzmann function as described previously (Hargus et al., 2011).

For steady-state inactivation, neurons were held at −120 mV and test potentials from −115 mV to −10 mV for 500 ms at 5 mV increments were applied. The second pulse to −10 mV for 40 ms was used to assess channel availability. Currents during the second pulse were normalized for each cell with the largest current as 1.0 and fit to the Boltzmann function.

I_{NaP} was determined in brain slice preparations using voltage ramps from −100 mV to −10 mV at a rate of 65 mV/s. I_{NaP} was recorded in bath solution containing the following (in mM): 30 NaCl, 120 TEA-Cl, 10 $NaHCO_3$, 1.6 $CaCl_2$, 2 $MgCl_2$, 0.2 $CdCl_2$, and 5 4-AP, 15 glucose, pH 7.4 when oxygenated with 95% O_2 and 5% CO_2; temperature 32°C, and a pipette solution containing the following (in mM): 140 CsF, 2 $MgCl_2$, 1 EGTA, 10 HEPES, 4 Na_2ATP, and 0.3 NaGTP, pH adjusted to 7.3 with CsOH, osmolarity adjusted to 310 MΩ with sucrose. Ramp voltage recordings displayed an inward current that was referred to as I_{NaP}. To determine the peak I_{NaP} current, voltage ramp protocols were repeated in the presence of TTX (1 μM). Traces obtained in the presence of TTX were subtracted from those obtained in its absence. TTX was reconstituted in ACSF.

I_{NaR} was also recorded in brain slice preparations using a bath solution containing the following (in mM): 100 NaCl, 26 $NaHCO_3$, 19.5 TEA-Cl, 3 KCl, 2 $MgCl_2$, 2 $CaCl_2$, 2 $BaCl_2$, 0.1 $CdCl_2$, 4 4-AP, and 10 glucose, pH 7.4 when oxygenated with 95% O_2 and 5% CO_2; temperature 32°C, using the same pipette solution as that for recording I_{NaP}. Neurons were held at −100 mV and depolarized to +20 mV for 20 ms, followed by either a single repolarizing step to −30 mV for 100 ms to determine the peak I_{NaR} or a series of repolarizing steps from −100 mV to −10 mV to determine the voltage dependence of I_{NaR}. Protocols were again repeated in the presence of TTX (1 μM) to determine I_{NaR} current amplitudes and gating.

Immunohistochemistry. WT, D/+, and D/D mice (minimum 3 mice for each genotype) were anesthesized with isoflurane, decapitated, and brains rapidly removed and placed in chilled (4°C) ACSF. Horizontal 500-μm-thick sections were prepared using a Vibratome and transferred to a chamber containing oxygenated ACSF at 37°C and incubated for 35 min. Slices were then embedded in optimal cutting temperature compound in cryomolds, snap-frozen on dry-ice-chilled isopentane, and kept on dry ice. Cryostat sections (16 μm) were prepared and thaw-mounted onto Superfrost Plus slides (Fisher Scientific) and stored at −80°C for no longer than 3 days before further processing. Slices were fixed in an ice-cold acetone–ethanol mixture for 5 min, air-dried, washed with KPBS, and then placed for 60 min in KPBS blocking solution (5% fish skin gelatin, 5% normal goat serum, 0.25% Triton X-100, and 0.65% w/v BSA), followed by incubation in blocking solution containing the pair of primary antibodies for 48 h at 4°C (rabbit anti-$Na_v1.6$, 1:500, Alomone Laboratories, catalog #ASC-009, RRID:AB_2040202), and monoclonal mouse anti-Ankyrin G (1:500, NeuroMab N106/36, catalog #MABN466, RRID:AB_10697718). The slides were then washed with KPBS, incubated in blocking solution containing a pair of secondary antibodies (Alexa Fluor 488-conjugated goat anti-mouse IgG catalog #A-11029, RRID:AB_2534088 and Alexa Fluor 555-conjugated goat anti-rabbit IgG catalog #A-21429, RRID:AB_2535850, both at 1:500, both Invitrogen). Slides were washed in KPBS, incubated in nuclear blue (1 drop/ml; Invitrogen), washed, air-dried, and coverslipped in Polymount (Polysciences).

Confocal images were captured of mEC layer II neurons using a Zeiss LSM 710 confocal microscope with a 63× oil-immersion objective and ZEN Zeiss LSM Imaging software. The settings of the laser intensities and image capture were initially optimized but then not changed during the scanning of the slides. Quantification and analysis was performed using ImageJ software (RRID: SCR_003070). For analysis of $Na_v1.6$ and Ankyrin G immunofluorescence intensity, a line scan representing the length of the AIS as determined by Ankyrin G labeling was drawn and the relative optical density (ROD) was determined along the duration of the AIS. To compare the localization of $Na_v1.6$ in the AIS between genotypes, plots of ROD along the duration of the AIS for $Na_v1.6$ and Ankyrin G were compared. $Na_v1.6$ expression was compared between genotypes by normalizing $Na_v1.6$ immunofluorescence against that of Ankyrin G for each AIS and the average $Na_v1.6$/Ankyrin G ratio was calculated to determine channel density.

Data analysis. Electrophysiology data analysis was performed using Clampfit software version 10 (Molecular Devices) and MATLAB (The MathWorks, RRID: SCR_001622). All values represent means ± SEM. Statistical significance was determined by using either a standard one-way or two-way ANOVA followed by Tukey's *post hoc* test for parametric data or the rank-sum test for nonparametric data (GraphPad Prism 6.02 software, RRID:SCR_002798).

Results

Aberrant spike frequency in mEC layer II stellate neurons

Membrane properties were recorded from visually identified mEC layer II stellate neurons (Fig. 1). In comparison with WT littermates, AP firing frequencies were significantly elevated in D/D and D/+ neurons at current injection steps of 110 pA and 120 pA (Fig. 1*D*,*E*). For example, at 110 pA, the AP firing rate was increased by >3-fold in D/+ neurons (7.6 ± 1.1 Hz, $n = 20$: $p < 0.05$) and by >4-fold in D/D neurons (9.6 ± 1.2 Hz, $n = 27$: $p < 0.05$) compared with WT neurons (2.2 ± 1.2 Hz, $n = 20$). At the higher depolarizing current injection steps, we recorded spike frequency adaptation in D/+ and D/D neurons, but not in WT neurons. For example, at 470 pA, the AP firing frequency was 35.9 ± 3.3 Hz ($n = 20$) in WT neurons and was reduced to 26.9 ± 3.2 Hz ($n = 27$: $p < 0.05$) in D/+ and 17.2 ± 1.9 Hz ($n = 20$: $p < 0.05$) in D/D neurons (Fig. 1*D–F*). Firing frequencies between D/D and D/+ neurons were only significantly different at current injection steps of 460 and 470 pA ($p < 0.05$; Fig. 1*F*).

Altered neuronal membrane properties

AP spikes elicited from D/+ and D/D neurons appeared distinct from WT neurons. To quantify the apparent differences in the elicited APs, we measured the membrane properties of the first three APs evoked at 290 pA, a stimulation intensity that evoked a similar frequency of APs (~21 Hz) in all genotypes (Fig. 2*Ai–Ci*). We measured the maximal negative repolarizing voltage between AP spikes (Fig. 2*E*). In WT neurons, the maximal hyperpolarizing voltages between AP spikes trended toward more negative voltages after the initial AP spike. For D/+ and D/D neurons, a greater depolarized interspike voltage was recorded immediately

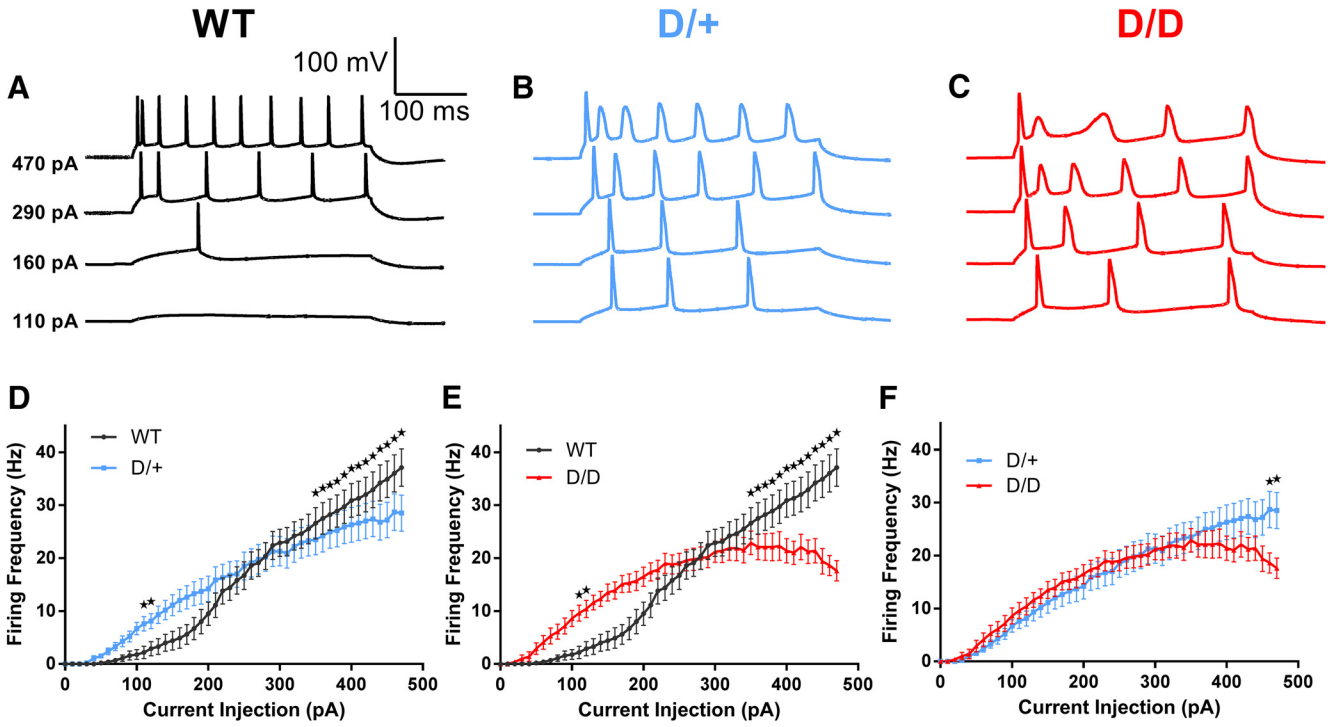

Figure 1. Neuronal hyperexcitability of mEC layer II stellate neurons from *Scn8a*^{N1768D} mice. ***A–C***, Representative traces of spikes elicited by 300 ms current injection steps of increasing current from a holding potential of −65 mV. ***D***, ***E***, Higher firing rates of D/+ ($n = 20$) and D/D ($n = 21$) neurons compared with WT ($n = 20$) at stimulation <300 pA. ***F***, Firing rate of D/+ neurons is greater than that of D/D neurons at stimulation >460 pA. Data are shown as means ± SEM. *$p < 0.05$, two-way ANOVA with *post hoc* Tukey's test for multiple comparisons.

after the first spike and remained significantly elevated for all subsequent spikes compared with WT ($p < 0.05$). In addition, D/D neurons showed a significantly depolarized interspike voltage compared with D/+ neurons ($p < 0.05$). These data suggest an increase in depolarizing current in mutant neurons that likely accounts for the increase in firing frequency seen with somatic current injection.

RMP and R_i did not differ between genotypes (Table 1). The threshold potential for the first AP was not affected by genotype, but that for the second and third APs was significantly depolarized in D/D neurons compared with WT. Within both the D/+ and D/D genotypes, the AP threshold was significantly depolarized in the second and third APs compared with first AP. In contrast, thresholds in WT neurons did not change with successive APs.

The amplitude of the first AP was elevated in D/+ and D/D neurons compared with WT (Fig. 2*D*, Table 1), but was reduced in the second AP for the mutant neurons. The amplitude of the third AP remained significantly reduced in D/D neurons compared with WT neurons. Within each genotype, WT neurons showed no significant changes in AP amplitude between the successive APs (Table 1). D/+ and D/D neurons showed a significant reduction in AP amplitude when comparing the first AP with the second and third AP spikes. However, when comparing the second and third AP spikes from mutant neurons, AP amplitudes of the third AP were significantly ($p < 0.05$) increased, likely due to the increase in interspike intervals, allowing recovery of some inactivated Na channels. The duration of all three APs measured at 50% (APD_{50}) and 90% (APD_{90}) was significantly increased in the mutant neurons compared with WT ($p < 0.05$: Fig. 2*D*, Table 1). In addition, APD_{50} and APD_{90} were significantly ($p < 0.05$) increased in D/D neurons compared with D/+ neurons for the second and third elicited APs. Within the D/+ and D/D genotypes, the durations of the second and third AP spikes were more prolonged than the first AP (Fig. 2*Bii*,*Cii*, Table 1). Again, no significant changes in AP duration for successive APs were detected in WT neurons.

A surprising finding was the slower upstroke velocities for the mutant APs compared with WT (Fig. 2*Bii*,*Cii*). When comparing within genotypes, the second and third AP spike upstroke velocities were significantly reduced compared with the first AP. Downstroke velocities in mutant neurons were also dramatically slower compared with WT cells for all three elicited APs (Fig. 2*Bii*,*Cii*). For all genotypes, downstroke velocity was significantly decreased in the second and third APs compared with the first AP.

Phase plots of the first three APs are shown in Figure 2, *Aiii–Ciii*. The inflections along the rising segment of the phase plots (arrows) result from the axonally initiated spike, which is followed by invasion into the soma and the activation of additional channels there (indicated with a plus sign). In WT neurons, the first inflection representing the AIS spike was less obvious and was continuous with the somatic inflection, suggesting an initiation site close to the soma and a smooth rapid invasion of the spike into the soma. In contrast, AIS inflections were more pronounced in D/+ and D/D neurons, suggesting disrupted backpropagation into the soma (Fig. 2*Aiii–Ciii*). Analysis of the first and second derivatives of the first AP evoked by current injection into the soma further emphasizes the presence of two prominent, but smaller peaks representing the AIS and somatic spikes in D/+ and D/D neurons (Fig. 2*Biv–Civ*). The latency between the two peaks (t_{del}) was measured from the second derivative and was significantly longer in both D/+ neurons (0.35 ± 0.02 ms $p < 0.05$; $n = 16$) and D/D neurons (0.42 ± 0.03 ms $p < 0.05$; $n = 17$) compared with WT neurons (0.05 ± 0.01 ms; $n = 15$). A delay in the axosomatic spike has been suggested previously to indicate a change in the spike initiation site to more distal sites from the

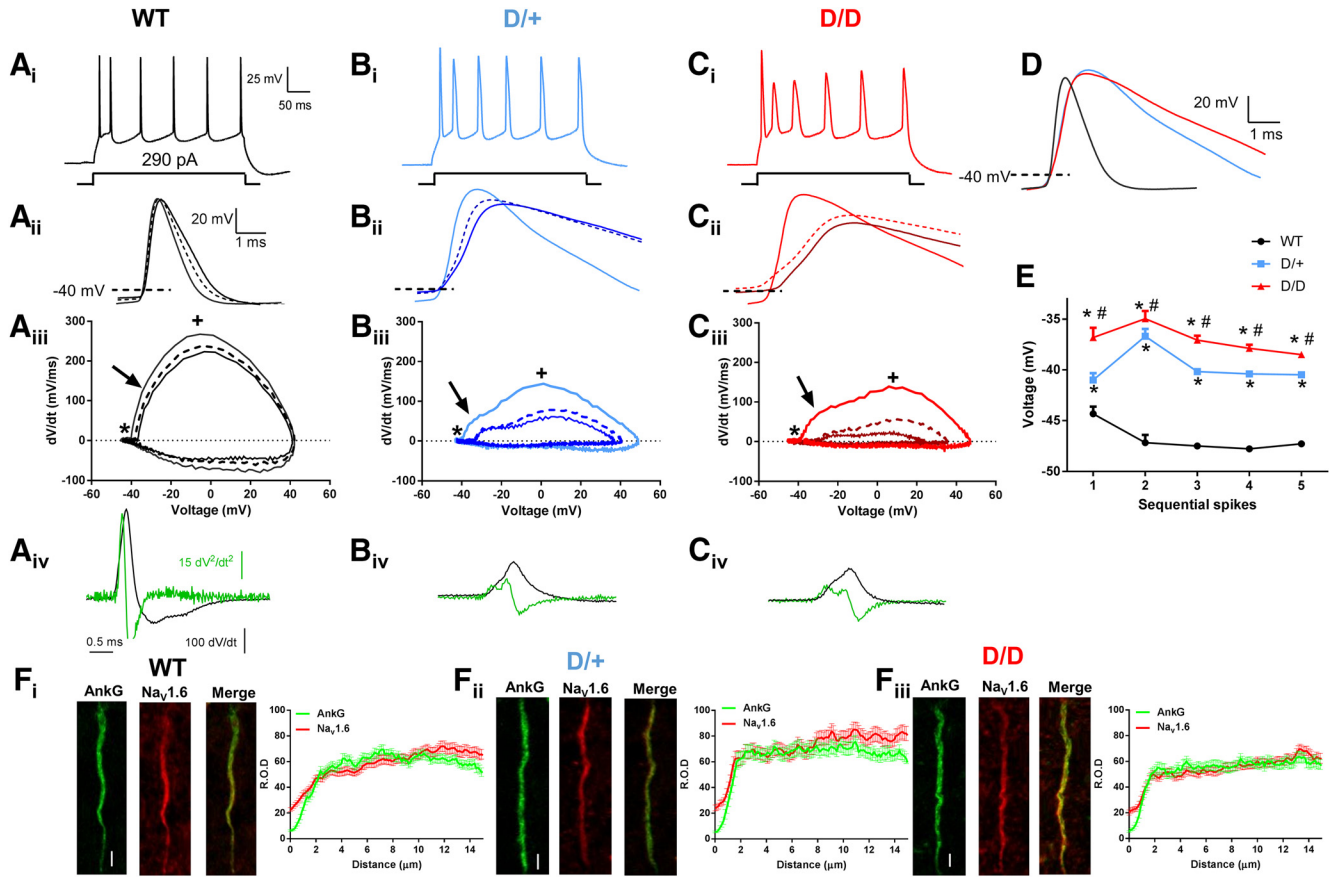

Figure 2. Aberrant AP morphology in mutant mEC neurons. ***Ai–Ci***, AP morphology elicited by a 300 ms depolarizing current injection of 290 pA. ***D***, Superimposition of the first AP spike elicited by a depolarizing step to 290 pA from WT, D/+, and D/D neurons demonstrating the increase in AP duration in mutant neurons compared with WT. Note the delay in rising and falling phase of the AP in D/+ and D/D neurons. ***Aii–Cii***, Superimposed traces of the first three AP spikes elicited by injection of 290 pA. The duration of spikes 2 and 3 is extended in the mutant neurons. Solid trace is the first AP, darker traces are the second AP, and broken lines are the third AP. ***Aiii–Ciii***, Phase plots of dV/dt vs voltage for the first three AP spikes. *AP thresholds. Arrow indicates inflection of the rising phase of the phase plot indicative of AIS spike initiation; +, maximal conduction velocity as the spike invades the soma. The abrupt rise of dV/dt seen in WT neurons is less pronounced for the first spike in mutant neurons and further slowed for the second and third spikes. ***Aiv–Civ***, First derivative (dV/dt) derived for the first AP spike. The peak of the first derivative is reduced in mutant neurons, indicating a slower upstroke velocity of the AP. Latency between spike initiation at the AIS and invasion into the soma was lengthened in mutant neurons, suggesting slower spike conduction. Second derivatives of the APs (superimposed, green) are also shown. The peaks are clearly discernable for the mutant neurons and are separated by a more pronounced latency. ***E***, Plot of maximal hyperpolarizing voltages between AP spikes evoked by a 290 pA current injection (WT, $n = 20$; D/+, $n = 20$; D/D, $n = 21$). ***Fi–Fiii***, Left, Na_v 1.6 expression along the AIS of WT, D/+, and D/D neurons (AnkG, green; Na_v1.6, red; Merge; yellow). Right, Graphs showing the localization and ROD of AnkG and Na_v1.6 (WT, $n = 124$ from 4 animals; D/+, $n = 83$ from 3 animals; D/D, $n = 100$ from 4 animals) staining along the length of the AIS for WT, D/+, and D/D neurons. Scale bars, 2 μm. Data are shown as mean ± SEM. *$p < 0.05$, one-way ANOVA with *post hoc* Tukey's test for multiple comparisons compared with WT; $^{\#}p < 0.05$ one-way ANOVA with *post hoc* Tukey test for multiple comparisons when D/+ were compared with D/D neurons.

Table 1. Membrane properties of WT, D/+, and D/D mEC layer II stellate neurons

	RMP, mV	R_i, MΩ	Threshold, mV	Amplitude, mV	APD_{50}, ms	APD_{90}, ms	Upstroke velocity, mV/ms	Downstroke velocity, mV/ms	*n*
1 st AP									
WT	−65.8 ± 1.1	111.8 ± 10.9	−40.4 ± 1.4	42.1 ± 1.7	0.8 ± 0.1	2.5 ± 0.1	268.0 ± 9.1	−77.5 ± 3.5	20
D/+	−66.1 ± 1.2	112.6 ± 11.2	−41.3 ± 4.2	47.3 ± 1.4[a]	2.5 ± 0.2[a]	7.1 ± 0.7[a]	190.2 ± 19.4[a]	−34.6 ± 2.2[a]	20
D/D	−65.7 ± 2.1	110.7 ± 13.2	−41.6 ± 1.2	46.4 ± 1.3[a]	3.3 ± 0.2[a,b]	9.6 ± 1.2[a]	168.6 ± 5.8[a,b]	−21.4 ± 2.7[a,b]	21
2 nd AP									
WT			−37.4 ± 0.9	40.9 ± 0.9	1.4 ± 0.1	2.9 ± 0.1	218.0 ± 10.2[c]	−48.6 ± 2.5[c]	20
D/+			−36.5 ± 1.1[c]	33.6 ± 2.9[a,c]	4.8 ± 0.8[a,c]	8.7 ± 0.7[a,c]	100.2 ± 22.0[a,c]	−19.2 ± 2.9[a,c]	20
D/D			−32.8 ± 1.8[a,c]	25.4 ± 0.9[a,b,c]	7.7 ± 0.5[a,b,c]	14.4 ± 1.2[a,b,c]	55.6 ± 7.1[a,b,c]	−12.8 ± 2.6[a,b,c]	21
3 rd AP									
WT			−37.9 ± 0.9	41.4 ± 2.7	1.3 ± 0.8	2.9 ± 0.2	229.7 ± 11.8[c]	−59.3 ± 1.2[c]	20
D/+			−35.9 ± 1.7[c]	38.3 ± 1.8[c,d]	5.2 ± 0.6[a,c]	9.7 ± 1.7[a,c]	98.5 ± 17.9[a,c]	−19.0 ± 1.9[a,c]	20
D/D			−31.1 ± 1.1[a,b,c]	32.9 ± 1.1[a,b,c,d]	8.2 ± 1.7[a,b,c]	14.1 ± 1.8[a,b,c]	53.7 ± 7.1[a,b,c]	−13.0 ± 3.5[a,b,c]	21

Values represent mean ± SEM. *n* = number of cells.

[a] $p < 0.05$ versus WT neurons.

[b] $p < 0.05$ D/+ versus D/D.

[c] $p < 0.05$ 1 st AP versus 2 nd and 3 rd APs within the same genotype.

[d] $p < 0.05$ 2 nd versus 3 rd AP within the same genotype.

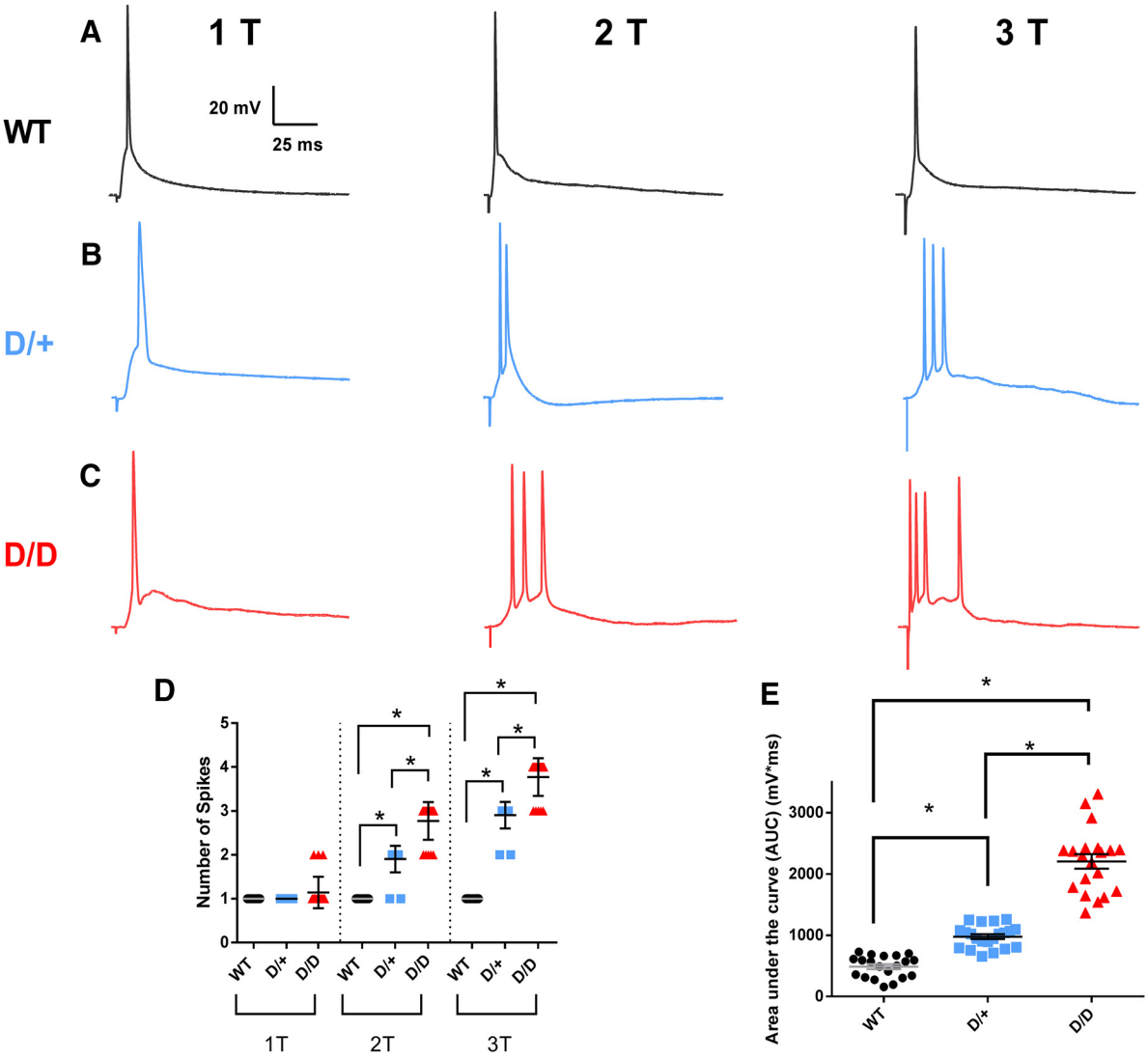

Figure 3. Synaptic stimulation of mutant mEC neurons elicits burst firing and prolonged depolarization. ***A–C***, mEC deep layers were briefly stimulated at the AP threshold (1T), at twice the threshold value (2T), and at three times the threshold (3T). AP firing was measured in WT ($n = 20$), D/+ ($n = 21$), and D/D neurons ($n = 22$). Bursts of APs were elicited in the mutant neurons in response to 2T and 3T stimulation. ***D***, AP frequency in response to increasing stimulation intensity. ***E***, AUC for APs evoked at 1T stimulation is greater for D/D neurons than for D/+ or WT neurons. Data are shown as mean ± SEM. *$p < 0.05$, one-way ANOVA with *post hoc* Tukey's test for multiple comparisons.

soma (Royeck et al., 2008). To determine whether $Na_v1.6$ expression along the AIS was different in the mutant neurons compared with WT, immunofluorescence experiments were performed (Fig. 2*Fi–Fiii*). Robust $Na_v1.6$ staining was observed at the AIS and was colocalized with Ankyrin G staining, a marker for the AIS. No differences in staining pattern were detected between any of the genotypes along the AIS, suggesting a similar expression profile of $Na_v1.6$ in all three genotypes.

Synaptically evoked AP bursting in N1768D mutant mice

Brief stimulation of the deep layers of the mEC evoked a single AP spike in mEC layer II stellate neurons of all three genotypes (1T; Fig. 3*A–C*). However, increasing the stimulation intensity above AP threshold to twofold (2T) or threefold (3T) evoked multiple AP spikes in D/+ neurons ($n = 21$) and D/D neurons ($n = 20$), but not in WT neurons ($n = 20$; Fig. 3*A–D*). Significantly more spikes were evoked in D/D neurons than in D/+ neurons ($p < 0.05$).

In addition to bursting, synaptically evoked responses produced longer depolarizations in D/+ and D/D neurons than in WT neurons. Analysis of evoked APs revealed an increase in the duration of the depolarizing event from 59.6 ± 5.9 ms ($n = 20$) in WT neurons to 110.7 ± 6.1 ms ($n = 21$: $p < 0.05$) in D/+ neurons and further to 176.1 ± 11.5 ms ($n = 20$: $p < 0.05$) in D/D neurons. The evoked responses in D/D neurons had significantly longer durations than those in D/+ neurons. Analysis of the area under the evoked response curve (AUC) at T1 revealed a 2-fold to 4-fold increase in D/+ neurons ($n = 21$: $p < 0.05$) and D/D neurons ($n = 20$: $p < 0.05$) compared with WT ($n = 20$) (Fig. 3*E*). D/D neurons also had a significant increase in AUC at T1 stimulation compared with D/+ cells ($p < 0.05$). Similar increases in mutant neurons were also seen at T2 and T3 stimulation (data not shown).

I_{NaP} and I_{NaR} currents are elevated in mutant neurons

I_{NaP} currents are thought to be major contributors to the generation of high-frequency AP firing. Elevated I_{NaP} has been recorded in neurons from human patients and animal models of epilepsy (Vreugdenhil et al., 2004; Stafstrom, 2007; Hargus et al., 2011, 2013) and the N1768D channel generates elevated persis-

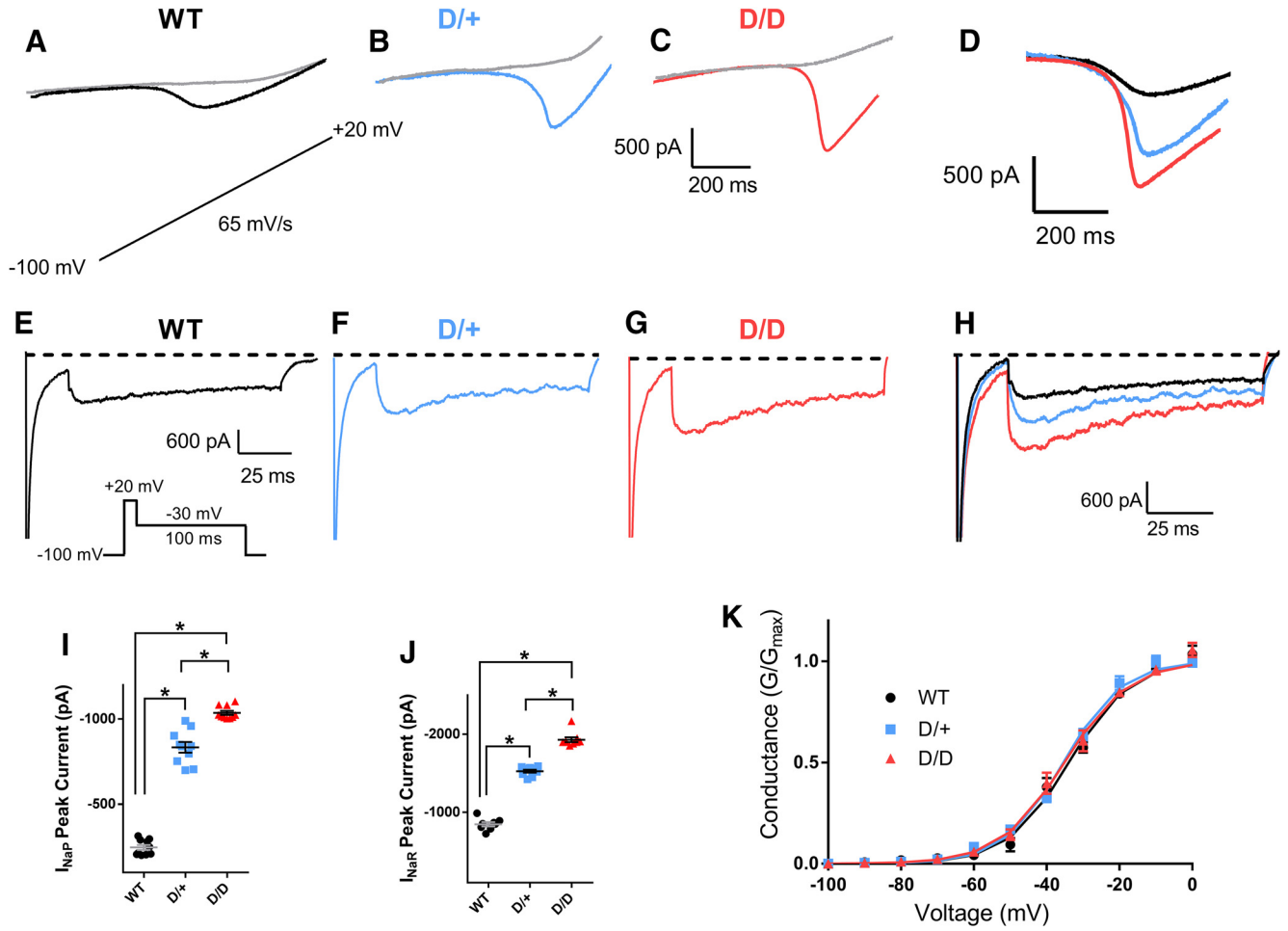

Figure 4. I_{NaP} and I_{NaR} Na channel currents are increased in N1768D mutant mEC layer II stellate neurons. Using recording solutions designed to reduce other types of inward and outward currents, voltage ramps were applied at a rate of 65 mV/s (inset) to elicit I_{NaP} currents. All I_{NaP} currents were abolished in the presence of 1 μM TTX (gray traces). Amplitudes of I_{NaP} currents were obtained by taking the original trace and subtracting from it the trace recorded in the presence of TTX (1 μM). ***A–C***, I_{NaP} recordings from WT, D/+, and D/D mEC neurons. ***D***, Superimposition of TTX subtracted I_{NaP} amplitudes for the three genotypes. ***E–G***, I_{NaR} recordings from WT, D/+, and D/D mEC neurons. I_{NaR} currents were recorded using the indicated voltage protocol. Traces shown were obtained after subtracting traces recorded in the presence of TTX (1 μM). ***H***, Superimposition of I_{NaR} of the three genotypes. ***I***, Peak I_{NaP} currents in WT ($n = 10$), D/+ ($n = 10$), and D/D ($n = 10$) mEC neurons. ***J***, Peak I_{NaR} currents in WT ($n = 8$), D/+ ($n = 9$), and D/D ($n = 9$) mEC neurons. ***K***, Voltage dependence of I_{NaR} activation revealed no significant shifts in $V_{1/2}$ or *k*. Smooth lines correspond to the least-squares fit when average data were fit to a single Boltzmann equation. Data are shown as mean ± SEM. *$p < 0.05$, one-way ANOVA with *post hoc* Tukey's test for multiple comparisons.

tent current in transfected cells (Veeramah et al., 2012) and in hippocampal neurons (Lopez-Santiago et al., 2017). To determine whether I_{NaP} currents were increased in mEC layer II stellate neurons from the N1768D mutant mice, voltage ramps were applied in brain slice preparations. Ramp voltage recordings displayed an inward current that was completely abolished by the application of 1 μM TTX (Fig. 4*A–C*). The peak I_{NaP} current amplitude was determined by subtracting traces obtained in the presence of TTX from those obtained in its absence. I_{NaP} currents in WT littermates had amplitudes of −247 ± 14 pA ($n = 10$). Amplitudes were significantly higher in both D/+ neurons (−834 ± 6 pA; $n = 10$: $p < 0.05$) and D/D neurons (−1037 ± 12 pA; $n = 10$: $p < 0.05$). I_{NaP} currents were larger in D/D than in D/+ neurons ($p < 0.05$) (Fig. 4*D*,*I*). Conductance plots of I_{NaP} currents revealed no significant differences in activation parameters (data not shown).

I_{NaR} currents are slow inactivating depolarizing currents that can contribute to increased AP frequency and burst firing (Raman and Bean, 1997). Peak I_{NaR} currents were significantly elevated in D/+ neurons (−1522 ± 22 pA; $n = 9$: $p < 0.05$) and D/D neurons (−1936 ± 34 pA; $n = 9$: $p < 0.05$) compared with WT (−847 ± 27 pA; $n = 10$; Fig. 4*E–H*,*J*). In a similar manner to I_{NaP} currents, I_{NaR} current amplitudes were also larger in D/D than in D/+ neurons ($p < 0.05$; Fig. 4*H*,*J*), demonstrating the greater deleterious effect of two copies of the mutant channel and the absence of WT channel. The properties of I_{NaR} activation were not altered in any of the mice (Fig. 4*K*).

Effects of TTX (30 nM) on I_{NaR} and I_{NaP} currents

Elevated I_{NaR} and I_{NaP} currents could account for increased firing frequencies, AP burst firing upon synaptic stimulation and greater depolarized inter spike voltages observed in D/+ and D/D neurons. Low concentrations of TTX have been shown to reduce spike afterdepolarized potentials (ADPs) without affecting properties of the fast spike (Yue et al., 2005). To test the specific contributions of I_{NaR} and I_{NaP} to the aberrant AP morphology observed in mutant neurons, we first determined the effects of 30 nM TTX on I_{NaR} and I_{NaP} currents (Fig. 5) and then determined the effects of reducing I_{NaR} and I_{NaP} currents on AP spikes (Fig. 6). TTX (30 nM) caused a small decrease in I_{NaP} peak current in WT neurons, but this did not reach significance (Fig. 5*A*,*D*). In contrast, TTX (30 nM) caused a significant reduction in both D/+

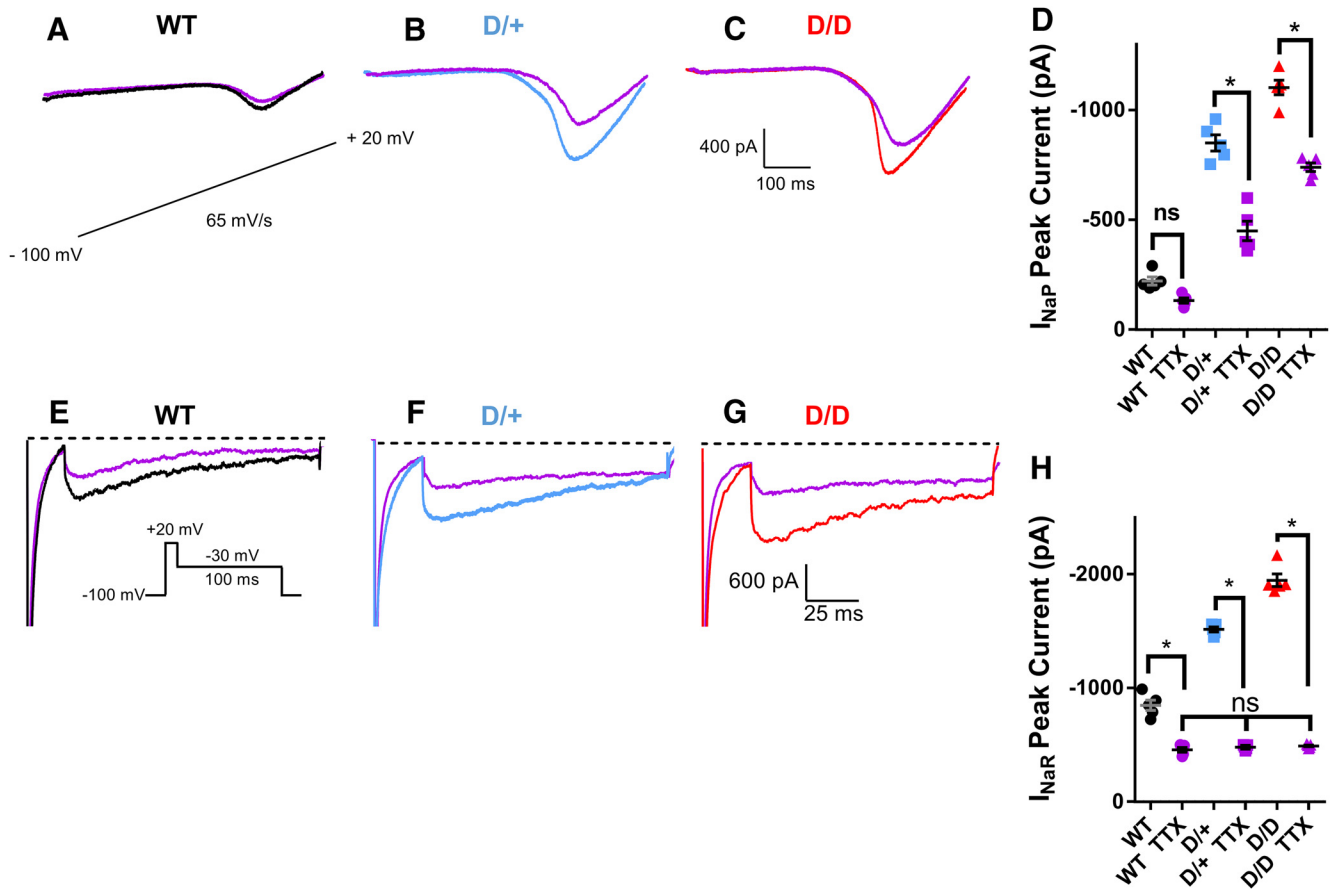

Figure 5. TTX (30 nM) decreases I_{NaP} and I_{NaR} currents. ***A–C***, I_{NaP} currents were elicited by applying a voltage ramp at a rate of 65 mV/s before (WT, black; D/+, blue; D/D, red) and after application of TTX (30 nM; purple traces for all genotypes). Traces shown are those obtained after subtracting traces recorded in the presence of TTX (1 μM). ***D***, Scatter plot of I_{NaP} peak amplitudes before and after the application of TTX (30 nM) (WT, $n = 5$; D/+, $n = 5$; D/D, $n = 5$). ***E–G***, I_{NaR} measured before (WT, black; D/+, blue; D/D, red) and after the application of TTX (30 nM; purple traces for all the genotypes). ***H***, Scatter plot of I_{NaR} current peak amplitude before and after the presence of TTX (30 nM) (WT, $n = 6$; D/+, $n = 6$; D/D, $n = 5$). Data are shown as mean ± SEM. *$p < 0.05$, one-way ANOVA with *post hoc* Tukey's test for multiple comparisons.

(by 47%) and D/D (by 35%) I_{NaP} peak currents (Fig. 5*B–D*). In the presence of TTX, I_{NaP} currents remained significantly ($p < 0.05$) increased in D/+ and D/D neurons compared with WT and between D/+ and D/D neurons ($p < 0.05$). For I_{NaR} currents, TTX (30 nM) significantly reduced I_{NaR} peak currents in all three genotypes ($p < 0.05$; Fig. 5*E–H*). In the presence of TTX, I_{NaR} currents were not significantly different between WT and mutant neurons.

Effects of TTX (30 nM) on AP spikes

To determine the effects of reducing I_{NaP} and I_{NaR} currents on AP spike properties, we applied low concentrations of TTX (30 nM) and examined APs evoked at a current injection step of 290 pA, a level in which all three genotypes fire spikes at the same frequency. TTX (30 nM) had no effect on AP firing frequency in WT or D/+ neurons, but did significantly increase firing frequency of D/D neurons at current injection steps at 460 and 470 pA, reducing the extent of spike frequency adaptation (data not shown). TTX also had no effect on WT AP spike properties (Table 2). In contrast, TTX resulted in a more negative maximal repolarizing voltage potential between AP spikes of D/+ and D/D neurons, but many voltage potentials remained significantly more depolarized than WT (Fig. 6*Bii*,*Cii*). Furthermore, TTX increased the upstroke and downstroke velocities of the first and second AP spikes elicited in D/+ and D/D mEC neurons, reducing AP duration (Fig. 6*Biii–Ciii*, Table 2). AP amplitudes were also increased in the second AP spike for both D/+ and D/D neurons. Phase plots of the effects of TTX on all three genotypes are shown in Figure 6, *Aiv–Civ*, where a small, but significant rescue of AP morphology can be seen in D/+ and D/D neurons.

Low-concentration TTX has been shown to reduce ADPs that drive spike bursting in CA1 neurons (Yue et al., 2005). We evoked AP spikes using a brief, 4 ms suprathreshold current injection pulse (Fig. 6*D–F*). In WT neurons, the brief pulse elicited a single AP spike. In contrast, the brief pulse elicited burst firing in D/+ and D/D neurons. TTX (30 nM) had no effect on AP spikes in WT neurons, but eliminated burst firing in D/+ and D/D neurons, resulting in only a single AP being elicited in response to stimulation. Analysis of the AUC for spikes evoked showed significant decreases after application of TTX (30 nM; Fig. 2*G*), further supporting a major role for Na channel currents in driving burst epileptiform activity in these neurons.

Altered Na channel physiology

Previous evaluation of N1768D in transfected cells overexpressing the mutant channel revealed altered Na channel gating properties (Veeramah et al., 2012). To determine whether these alterations are seen when the mutant channel is expressed at a physiological level in neurons, Na channel currents were recorded using outside-out patches from visually identified mEC layer II stellate neurons in brain slice preparations (Fig. 7). Representative macroscopic Na currents are shown in Figure 7*A*. Na

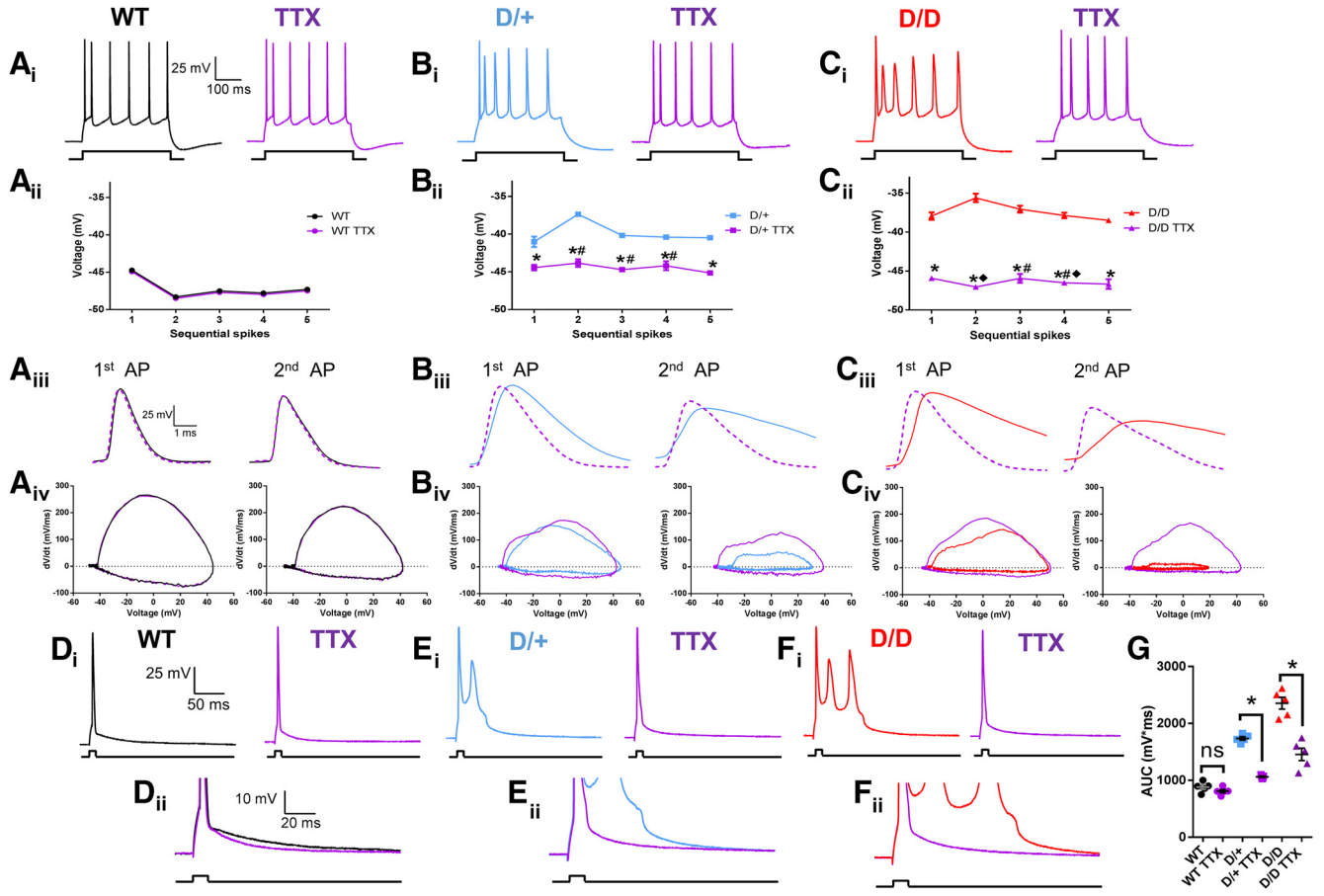

Figure 6. TTX (30 nM) increases upstroke velocity and decreases AP duration in D/+ and D/D neurons. ***Ai–Ci***, APs elicited by a 300 ms current injection pulse of 290 pA before (WT, black; D/+, blue; D/D, red) and after application of TTX (30 nM; purple traces for all genotypes). ***Aii–Cii***, Plot of maximal hyperpolarizing voltages between AP spikes evoked by a 290 pA current injection before and after the application of TTX (30 nM) (WT, $n = 10$; D/+, $n = 11$; D/D, $n = 13$). ***Aiii–Ciii***, Superimposed traces of the first two AP spikes elicited by injection of 290 pA (WT, black; D/+, blue; D/D, red) and after application of TTX (30 nM; purple traces for all genotypes). ***Aiv–Civ***, Superimposed phase plots of the first two elicited APs before (WT, black; D/+, blue; D/D, red) and after application of TTX (30 nM; purple traces for all genotypes). ***Di–Fi***, AP spikes elicited by a brief (4 ms) injection of suprathreshold current injection before (WT, black; D/+, blue; D/D, red) and after application of TTX (30; purple traces for all genotypes). ***Dii–Fii***, Superimposed traces of AP spikes shown in ***Di–Fi***. ***G***, Scatter plot showing the AUC for AP spikes elicited by a brief (4 ms) current injection pulse before and after the application of TTX (30 nM) (WT, $n = 5$; D/+, $n = 5$; D/D, $n = 5$). Data are shown as mean ± SEM. *$p < 0.05$, one-way ANOVA with *post hoc* Tukey's test for multiple comparisons comparing with the pre-TTX condition. ◆ $p < 0.05$, one-way ANOVA with *post hoc* Tukey's test for multiple comparisons comparing D/D + TTX with D/+ + TTX. #$p < 0.05$, one-way ANOVA with *post hoc* Tukey's test for multiple comparisons comparing WT + TTX.

Table 2. Effects of TTX (30 nM) on AP spikes

	RMP, mV	R_i, MΩ	Threshold, mV	Amplitude, mV	APD_{50}, ms	APD_{90}, ms	Upstroke velocity, mV/ms	Downstroke velocity, mV/ms	*n*
1st AP									
WT	−66.9 ± 1.1	113.8 ± 11.2	−41.3 ± 1.3	43.5 ± 1.8	1.1 ± 0.2	2.4 ± 0.5	266.0 ± 7.0	−78.1 ± 1.2	10
+TTX	−65.3 ± 2.1	109.8 ± 10.2	−42.0 ± 1.0	44.0 ± 1.7	1.2 ± 0.1	2.3 ± 0.2	262.9 ± 2.8	−75.3 ± 1.9	10
D/+	−65.1 ± 1.0	110.4 ± 10.2	−42.6 ± 5.5	46.3 ± 1.5	2.8 ± 0.5	7.8 ± 0.2	185.5 ± 5.5	−40.5 ± 1.2	11
+TTX	−65.4 ± 1.0	114.6 ± 12.1	−43.5 ± 1.2	45.5 ± 0.8	1.9 ± 0.1[a]	4.5 ± 0.5[a]	199.0 ± 2.1[a]	−51.2 ± 1.0[a]	11
D/D	−64.8 ± 1.2	111.8 ± 12.2	−40.9 ± 1.0	47.1 ± 2.1	4.0 ± 1.0	10.8 ± 0.1	156.8 ± 1.3	−20.1 ± 1.7	13
+TTX	−65.8 ± 1.2	109.7 ± 9.2	−42.0 ± 2.1	46.9 ± 2.1	2.7 ± 0.1[b]	6.5 ± 1.0[b]	198.1 ± 1.1[b]	−41.1 ± 1.0[b]	13
2nd AP									
WT			−38.2 ± 1.0	41.0 ± 0.9	1.6 ± 0.5	3.0 ± 1.2	210.2 ± 5.2	−44.9 ± 1.0	10
+TTX			−38.5 ± 1.5	41.2 ± 1.9	1.5 ± 0.2	3.1 ± 0.3	209.9 ± 7.2	−43.8 ± 1.2	10
D/+			−35.5 ± 2.6	30.9 ± 1.0	4.0 ± 0.5	9.5 ± 1.3	99.1 ± 12.0	−18.3 ± 0.5	11
+TTX			−37.5 ± 1.9	38.9 ± 1.0[a]	2.7 ± 0.1[a]	7.0 ± 1.1[a]	150.1 ± 8.0[a]	−29.0 ± 0.8[a]	11
D/D			−30.8 ± 1.2	22.1 ± 1.8	6.5 ± 1.3	16.8 ± 1.4	45.9 ± 1.9	−10.9 ± 0.5	13
+TTX			−36.8 ± 1.0[b]	38.1 ± 2.3[b]	3.5 ± 0.3[b]	8.5 ± 0.4[b]	142.9 ± 2.6[b]	−20.9 ± 0.3[b]	13

Values represent mean ± SEM. *n* = number of cells.

[a] $p < 0.05$ D/+ versus D/+ in presence of 30 nm TTX.

[b] $p < 0.05$ D/D versus D/D in presence of 30 nm TTX.

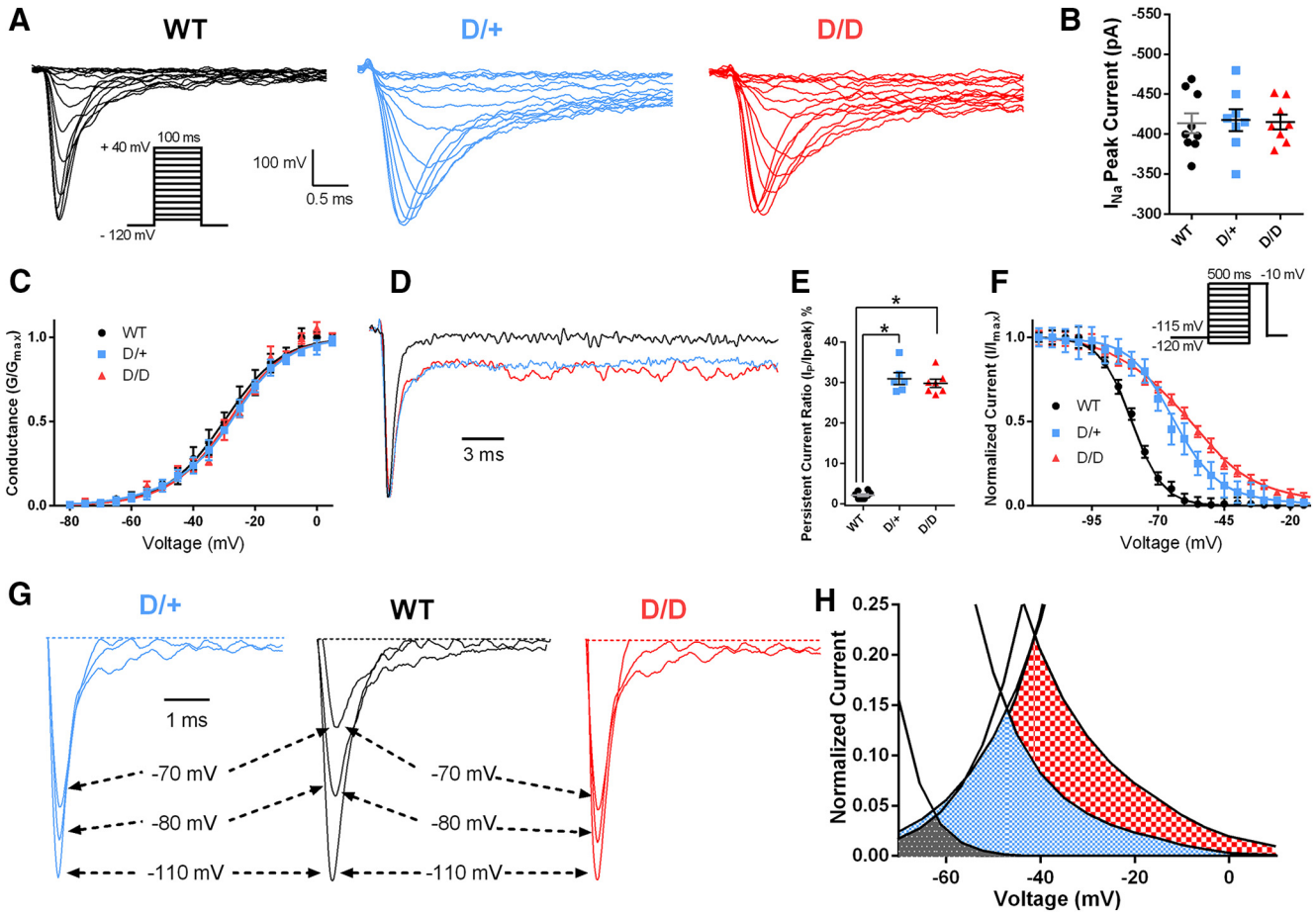

Figure 7. Altered Na channel currents in mutant mEC neurons. ***A***, Representative current traces recorded using the outside-out patch-clamp configuration for WT, D/+, and D/D mEC layer II stellate neurons. ***B***, Scatter plot of peak I_{Na} current from WT ($n = 9$), D/+ ($n = 8$), and D/D ($n = 8$) mEC neurons. ***C***, Voltage dependence of channel activation for WT ($n = 9$), D/+ ($n = 7$), and D/D ($n = 6$) mEC neurons. Lines correspond to the least-squares fit when average data were fit to a single Boltzmann equation. ***D***, Representative normalized current traces recorded during a 100 ms depolarizing pulse from a holding potential of −120 mV to −10 mV demonstrates elevated persistent Na current in mutant neurons. ***E***, Ratio of $I_{Persistent}/I_{peak}$ current 100 ms after stimulation in WT ($n = 9$), D/+ ($n = 7$), and D/D ($n = 6$) mEC neurons. ***F***, Voltage dependence of channel inactivation for WT ($n = 7$), D/+ ($n = 7$), and D/D ($n = 9$) neurons. Lines correspond to the least-squares fit when average data were fit to a single Boltzmann equation. ***G***, Representative steady-state inactivation traces elicited after prepulses to −110 mV, −80 mV, and −70 mV. Note the delay in channel inactivation for D/+ and D/D neurons compared with WT, indicating severe impairment of channel inactivation. ***H***, Window current obtained by overlapping normalized activation and inactivation curves. Window current is elevated in D/+ (blue shaded area) and D/D (red checkered area) compared with WT (black shaded area) neurons. The voltage range for the window current is also shifted in a depolarizing direction. Data are shown as mean ± SEM. *$p < 0.05$, one-way ANOVA with *post hoc* Tukey's test for multiple comparisons.

Table 3. Na channel physiology in WT, D/+, and D/D mEC layer II stellate neurons

	Activation			Inactivation			Persistent current	
	$V_{1/2}$	k	n	$V_{1/2}$	k	n	Ratio ($I_{persistent}/I_{peak}$)%	n
WT	−30.4 ± 1.4	−7.3 ± 0.2	9	−75.5 ± 1.5	6.1 ± 0.3	7	1.1 ± 0.5	9
D/+	−31.0 ± 2.3	−7.8 ± 0.7	7	−62.6 ± 2.3[a]	13.5 ± 1.3[a]	7	31.1 ± 0.5[a]	7
D/D	−30.5 ± 1.4	−7.9 ± 0.4	6	−58.2 ± 1.9[a,b]	17.6 ± 1.3[a,b]	9	32.1 ± 0.1[a]	6

Values represent mean ± SEM. n = number of cells.

[a]$p < 0.05$ versus WT.

[b]$p < 0.05$ D/+ versus D/D neurons.

channel current densities from outside-out recordings were not significantly different between genotypes (Fig. 7*B*). Analysis of *I–V* curves revealed no significant shifts in the voltage at half-maximal activation ($V_{1/2}$) or the slope factor (k) (Fig. 7*C*, Table 3). A frequent feature of $Na_v1.6$ gain-of-function mutations is the presence of a persistent/noninactivating Na current after prolonged depolarizations (Veeramah et al., 2012; Wagnon and Meisler, 2015; Wagnon et al., 2016; Meisler et al., 2016). Both D/+ and D/D neurons had significantly elevated persistent/noninactivating Na channel currents after a prolonged depolarization step from −100 mV to −10 mV for 100 ms (Fig. 7*D*,*E*, Table 3).

In contrast to the normal activation gating parameters, a significant depolarizing shift in the $V_{1/2}$ of steady-state inactivation was detected in D/+ (12.9 mV) and D/D (17.3 mV) neurons compared with WT (Fig. 7*F*,*G*, Table 3). k was also significantly increased in D/+ and D/D neurons (Table 3). Window currents were determined from the area under the overlapping normalized activation and inactivation curves (Fig. 7*H*). Window currents for D/+ and D/D neurons were increased by 7-fold and

12-fold, respectively, and were persistent over a greater voltage range than WT.

Discussion

In this study, we investigated the mechanisms by which the $Na_v1.6$ gain-of-function mutation N1768D leads to neuronal hyperexcitability, the hallmark of spontaneous seizures. Our studies reveal several new findings. First, we show that mEC layer II stellate neurons in D/+ and D/D mice are hyperexcitable, firing a greater number of AP spikes upon current injection than WT littermates, which is not the case for hippocampal or neocortical neurons (Lopez-Santiago et al., 2017). For D/+ mice, the increase in excitability of mEC neurons precedes the onset of seizures by >1 month.

Second, AP spike morphology was strikingly aberrant in D/+ and D/D mEC neurons, a finding that was not observed when the mutation was overexpressed in cultured hippocampal neurons (Veeramah et al., 2012) or in CA3 and cortex layer 2/3 neurons of D/+ mice (Lopez-Santiago et al., 2017). The most obvious abnormality was the increased spike width and slower upstroke velocity in mutant neurons. Sodium entry occurs mainly during the upstroke of the AP, with much less entry during the repolarization phase (Carter and Bean, 2009). The incomplete Na channel inactivation during the falling phase of the AP in mutant neurons would have three effects: (1) continued Na entry into the cell, increasing as the membrane potential moved further from the equilibrium potential for Na and thus providing a sustained depolarizing current during spike trains; (2) opposition to repolarizing potassium currents, thus lengthening the refractory period; and (3) accumulation of inactivated Na channels with subsequent spikes as a result of a greater depolarized interspike voltages. We report here that AP duration was significantly increased in both D/+ and D/D mEC neurons compared with WT, a finding that was also seen in CA1 neurons, but not in CA3 or neocortex neurons (Lopez-Santiago et al., 2017). Application of low-concentration TTX (30 nM) significantly reduced the interspike repolarization voltages, increased upstroke velocity, and reduced AP duration in mutant neurons. A likely explanation for these observations is that block of Na channel currents, particularly I_{NaP} and I_{NaR} currents, reduces persistent depolarizing current, hyperpolarizes the interspike voltage potentials, and allows recovery of Na channels inactivated after the first spike. These channels would be available and contribute to increasing upstroke velocity of the second and third spikes. A reduction in the depolarizing Na current due to TTX inhibition would also provide less opposition to repolarizing potassium currents, further enhancing repolarization and reducing AP duration.

Third, we show for the first time that neuronal resurgent (I_{NaR}) currents are increased as a result of the gain-of-function mutation in $Na_v1.6$. I_{NaR} currents are slow-inactivating currents that contribute to enhanced firing frequency and the generation of burst firing. I_{NaR} currents generate strong regenerative depolarizing currents that contribute to elevated spike frequency (Raman and Bean, 1997; Yue et al., 2005). Increased I_{NaR} currents are predicted to provide excessive depolarizing current that would significantly increase the firing frequency of mutant neurons and the excitatory drive into neuronal circuits (Yamada-Hanff and Bean, 2013). An increase in I_{NaR} currents was recently reported in cultured cells expressing two missense mutations of $Na_v1.6$, including N1768D (Patel et al., 2016), further supporting the importance of this current in epilepsy.

We evoked APs either by somatic depolarization or stimulation of presynaptic inputs. Somatic depolarization caused premature AP initiation and increased frequency of AP firing at lower current injection steps in mutant neurons. At greater depolarizations, a reduction in AP frequency was observed in the mutant neurons, likely due to an accumulation of noninactivating Na channels and the impaired recovery of completely inactivated channels as interspike membrane voltages remained depolarized. In support of this, low concentrations of TTX (30 nM) increased firing frequencies of D/D neurons at high stimulation intensities (460 and 470 pA). A surprising finding was the similar firing frequency of D/+ and D/D neurons except at very high current injection levels, where adaptation was more pronounced in D/D neurons. This was unexpected because I_{NaP} and I_{NaR} currents recorded from the soma were larger in D/D than in D/+ neurons and the greater rightward shift in the inactivation curve produced larger window currents in D/D neurons. Together, these events significantly increase the availability of a depolarizing current for spike initiation at earlier depolarizing steps in D/D neurons. However, a consequence of sustained depolarizations at greater depolarizing steps is the increase in the proportion of completely inactivated Na channels that would limit Na channel availability for spike initiation at high firing frequencies. In contrast, synaptically evoked responses were significantly different, with D/D neurons evoking longer depolarizing events and greater bursts of AP spikes than D/+ neurons. WT neurons fired only single spikes even at high stimulation intensities. The presence of mutant $Na_v1.6$ channels in dendrites (Caldwell et al., 2000) may account for these differences. Activation of the inactivation-deficient mutant channel along dendrites would amplify synaptic events, initiating regenerative spikes and increasing the probability of reaching spike threshold at the AIS.

A striking feature of neurons expressing the $Na_v1.6$ gain-of-function mutation is the profound increase in I_{NaP} and I_{NaR}, both of which are important in the regulation of firing frequency and burst firing (Raman and Bean, 1997; Yue et al., 2005). Increases in I_{NaP} and I_{NaR} have been reported in neurons from human patients (Vreugdenhil et al., 2004) and animal models of acquired epilepsy (Hargus et al., 2011, 2013). Several studies of EIEE13 mutations in cultured cells reported increased noninactivating persistent Na current after prolonged depolarizations (Veeramah et al., 2012; Estacion et al., 2014; Wagnon et al., 2016). Increased persistent currents were recently reported in hippocampal inhibitory and excitatory neurons of D/+ mice (Lopez-Santiago et al., 2017). We observed a clear, sustained increase in persistent current after prolonged depolarization of mutant neurons. An increase in I_{NaP} and I_{NaR} currents could cause proexcitatory changes in AP morphology, driving intrinsic bursting and sus-

Table 4. Different effects of the SCN8A-N1768D mutation in three classes of excitatory neurons

	mEC	CA1	CA3	Cortex 2/3
I_{NaP}	↑	↑	↑	ND
I_{NaR}	↑	ND	ND	ND
Inactivation $V_{1/2}$	↑	=	=	=
Maximum firing frequency	↑	↓	=	=
Synaptic evoked	↑	ND	ND	ND
Spontaneous firing	=	↑	↑	=
Upstroke velocity	↓	=	=	=
AP amplitude	↑	=	=	=
AP threshold	↓	=	=	=
AP duration	↑	↑	=	=

Properties of heterozygous mutant neurons are compared with WT cells. Hippocampal and cortical layer 2/3 data are from Lopez-Santiago et al. (2017).

↑, Increased; ↓, decreased; =, not changed; ND, not done.

taining neuronal hyperexcitability in mutant mice. Low concentrations of TTX inhibited both I_{NaP} and I_{NaR} and ameliorated abnormal AP morphology in D/+ and D/D neurons, as well as inhibiting AP burst firing elicited by brief stimulation pulses. These findings further support the importance of these currents in driving spike bursting (Yue et al., 2005).

We focused on mEC layer II stellate neurons because of their role in the excitation of hippocampal neurons. They have also been implicated in the initiation and propagation of epileptic seizures in models of temporal lobe epilepsy (Kobayashi et al., 2003). We observed profound proexcitatory alterations in mEC neurons, including increased spike amplitudes, slower upstroke velocities, and depolarizing shifts in Na channel inactivation parameters, all of which were not reported in hippocampal or neocortical neurons (Lopez-Santiago et al., 2017), further supporting brain region- and circuit-level specificity of the effects of this gain-of-function mutation. The properties of four classes of excitatory neurons from the D/+ mouse are compared in Table 4. Because mEC neurons relay excitatory inputs to the dentate gyrus and CA3 via the perforant and temporoammonic pathways (Witter et al., 1989), increased spiking frequency of mEC neurons would provide excessive excitatory input into the dentate gyrus and CA3 and further exacerbate an already hyperexcitable hippocampal circuit (Kobayashi et al., 2003).

The axon initial segment is the site of AP initiation (Rasband, 2010). During early mouse development, the AIS is first occupied by $Na_v1.2$, which is replaced by $Na_v1.6$ between 2 and 3 weeks of age (Boiko et al., 2001). This developmental profile may account for the onset of seizures in D/D mice at 3 weeks of age. Seizure onset in patients with *SCN8A* mutations ranges from 0 to 18 months and *in utero* seizures have been reported, suggesting that human $Na_v1.6$ may populate the AIS before birth (Singh et al., 2015).

A surprising finding was the observation of proexcitatory alterations in mEC neurons from D/+ mice more than a month before the onset of seizures. The delay may be explained by a requirement for activation of additional neurons and circuits that require additional time to mature into an epileptic state. Alternatively, seizure onset may require the higher levels of I_{NaP}, I_{NaR}, and window currents in mEC neurons that occur earlier in D/D mice to prime the epileptic circuit for seizure initiation. Further studies to explore epileptogenic circuits and key sites of seizure onset in this model of EIEE13 will be informative.

The N1768D mutation was identified in a heterozygous individual with EIEE13 and was first characterized using ND7/23 cells and cultured hippocampal neurons (Veeramah et al., 2012). We demonstrate that mutant neurons from the knock-in mouse model exhibit several of the abnormalities described in the transfected cells, including impaired channel inactivation, increased persistent current, and elevated firing rates. Our studies also provide new mechanistic information. The significant increases in two major Na channel currents critical in controlling neuronal excitability, I_{NaP} and I_{NaR}, add to the accumulating evidence of the importance of these currents in the pathology of the disease. We provide evidence of early proepileptiform behavior of mEC layer II stellate neurons in EIEE13. Because these proexcitatory changes precede the onset of spontaneous seizures in heterozygous mice, we propose that early neuronal hyperexcitability gradually increases the excitability of key cerebral circuits, culminating in the initiation of spontaneous seizures in this model of *SCN8A* encephalopathy.

References

Barker BS, Ottolini M, Wagnon JL, Hollander RM, Meisler MH, Patel MK (2016) The SCN8A encephalopathy mutation p.Ile1327Val displays elevated sensitivity to the anticonvulsant phenytoin. Epilepsia 57:1458–1466. CrossRef Medline

Blumenfeld H, Lampert A, Klein JP, Mission J, Chen MC, Rivera M, Dib-Hajj S, Brennan AR, Hains BC, Waxman SG (2009) Role of hippocampal sodium channel Nav1.6 in kindling epileptogenesis. Epilepsia 50:44–55. CrossRef Medline

Boiko T, Rasband MN, Levinson SR, Caldwell JH, Mandel G, Trimmer JS, Matthews G (2001) Compact myelin dictates the differential targeting of two sodium channel isoforms in the same axon. Neuron 30:91–104. CrossRef Medline

Caldwell JH, Schaller KL, Lasher RS, Peles E, Levinson SR (2000) Sodium channel Na(v)1.6 is localized at nodes of ranvier, dendrites, and synapses. Proc Natl Acad Sci U S A 97:5616–5620. CrossRef Medline

Carter BC, Bean BP (2009) Sodium entry during action potentials of mammalian neurons: incomplete inactivation and reduced metabolic efficiency in fast-spiking neurons. Neuron 64:898–909. CrossRef Medline

Estacion M, O'Brien JE, Conravey A, Hammer MF, Waxman SG, Dib-Hajj SD, Meisler MH (2014) A novel de novo mutation of SCN8A (Nav1.6) with enhanced channel activation in a child with epileptic encephalopathy. Neurobiol Dis 69:117–123. CrossRef Medline

Hammer MF, Wagnon JL, Mefford HC, Meisler MH (2016) SCN8A-related epilepsy with encephalopathy. Available from: http://www.ncbi.nlm.nih.gov/pubmed/27559564. Accessed July 20, 2016.

Hargus NJ, Merrick EC, Nigam A, Kalmar CL, Baheti AR, Bertram EH 3rd, Patel MK (2011) Temporal lobe epilepsy induces intrinsic alterations in Na channel gating in layer II medial entorhinal cortex neurons. Neurobiol Dis 41:361–376. CrossRef Medline

Hargus NJ, Nigam A, Bertram EH 3rd, Patel MK (2013) Evidence for a role of Nav1.6 in facilitating increases in neuronal hyperexcitability during epileptogenesis. J Neurophysiol 110:1144–1157. CrossRef Medline

Hu W, Tian C, Li T, Yang M, Hou H, Shu Y (2009) Distinct contributions of Na(v)1.6 and Na(v)1.2 in action potential initiation and backpropagation. Nat Neurosci 12:996–1002. CrossRef Medline

Jones JM, Meisler MH (2014) Modeling human epilepsy by TALEN targeting of mouse sodium channel Scn8a. Genesis 52:141–148. CrossRef Medline

Kaplan MR, Cho MH, Ullian EM, Isom LL, Levinson SR, Barres BA (2001) Differential control of clustering of the sodium channels Nav1.2 and Nav1.6 at developing CNS nodes of Ranvier. Neuron 30:105–119. CrossRef Medline

Kearney J, Plummer N, Smith M, Kapur J, Cummins T, Waxman S, Goldin A, Meisler M (2001) A gain-of-function mutation in the sodium channel gene Scn2a results in seizures and behavioral abnormalities. Neuroscience 102:307–317. CrossRef Medline

Kobayashi M, Wen X, Buckmaster PS (2003) Reduced inhibition and increased output of layer II neurons in the medial entorhinal cortex in a model of temporal lobe epilepsy. J Neurosci 23:8471–8479. Medline

Kong W, Zhang Y, Gao Y, Liu X, Gao K, Xie H, Wang J, Wu Y, Zhang Y, Wu X, Jiang Y (2015) SCN8A mutations in Chinese children with early onset epilepsy and intellectual disability. Epilepsia 56:431–438. CrossRef Medline

Larsen J, et al. (2015) The phenotypic spectrum of SCN8A encephalopathy. Neurology 84:480–489. CrossRef Medline

Levin SI, Khaliq ZM, Aman TK, Grieco TM, Kearney JA, Raman IM, Meisler MH (2006) Impaired motor function in mice with cell-specific knockout of sodium channel Scn8a (NaV1.6) in cerebellar purkinje neurons and granule cells. J Neurophysiol 96:785–793. CrossRef Medline

Lopez-Santiago LF, Yuan Y, Wagnon JL, Hull JM, Frasier CR, O'Malley HA, Meisler MH, Isom LL (2017) Neuronal hyperexcitability in a mouse model of SCN8A epileptic encephalopathy. Proc Natl Acad Sci U S A 114:2383–2388. CrossRef Medline

Lorincz A, Nusser Z (2008) Cell-type-dependent molecular composition of the axon initial segment. J Neurosci 28:14329–14340. CrossRef Medline

Martin MS, Tang B, Papale LA, Yu FH, Catterall WA, Escayg A (2007) The voltage-gated sodium channel Scn8a is a genetic modifier of severe myoclonic epilepsy of infancy. Hum Mol Genet 16:2892–2899. CrossRef Medline

Meisler MH, et al. (2016) SCN8A encephalopathy: research progress and prospects. Epilepsia 57:1027–1035. CrossRef Medline

Patel RR, Barbosa C, Brustovetsky T, Brustovetsky N, Cummins TR (2016) Aberrant epilepsy-associated mutant Nav1.6 sodium channel activity can be targeted with cannabidiol. Brain 139:2164–2181. CrossRef Medline

Raman IM, Bean BP (1997) Resurgent sodium current and action potential formation in dissociated cerebellar Purkinje neurons. J Neurosci 17: 4517–4526. Medline

Rasband MN (2010) The axon initial segment and the maintenance of neuronal polarity. Nat Rev Neurosci 11:552–562. CrossRef Medline

Royeck M, Horstmann MT, Remy S, Reitze M, Yaari Y, Beck H (2008) Role of axonal NaV1.6 sodium channels in action potential initiation of CA1 pyramidal neurons. J Neurophysiol 100:2361–2380. CrossRef Medline

Singh R, Jayapal S, Goyal S, Jungbluth H, Lascelles K (2015) Early-onset movement disorder and epileptic encephalopathy due to de novo dominant SCN8A mutation. Seizure 26:69–71. CrossRef Medline

Stafstrom CE (2007) Persistent Sodium Current and Its Role in Epilepsy. Epilepsy Curr 7:15–22. CrossRef Medline

Vacher H, Mohapatra DP, Trimmer JS (2008) Localization and targeting of voltage-dependent ion channels in mammalian central neurons. Physiol Rev 88:1407–1447. CrossRef Medline

Veeramah KR, O'Brien JE, Meisler MH, Cheng X, Dib-Hajj SD, Waxman SG, Talwar D, Girirajan S, Eichler EE, Restifo LL, Erickson RP, Hammer MF (2012) De novo pathogenic SCN8A mutation identified by whole-genome sequencing of a family quartet affected by infantile epileptic encephalopathy and SUDEP. Am J Hum Genet 90:502–510. CrossRef Medline

Vreugdenhil M, Hoogland G, van Veelen CW, Wadman WJ (2004) Persistent sodium current in subicular neurons isolated from patients with temporal lobe epilepsy. Eur J Neurosci 19:2769–2778. CrossRef Medline

Wagnon JL, Meisler MH (2015) Recurrent and non-recurrent mutations of SCN8A in epileptic encephalopathy. Front Neurol 6:104. CrossRef Medline

Wagnon JL, Korn MJ, Parent R, Tarpey TA, Jones JM, Hammer MF, Murphy GG, Parent JM, Meisler MH (2015) Convulsive seizures and SUDEP in a mouse model of SCN8A epileptic encephalopathy. Hum Mol Genet 24: 506–515. CrossRef Medline

Wagnon JL, Barker BS, Hounshell JA, Haaxma CA, Shealy A, Moss T, Parikh S, Messer RD, Patel MK, Meisler MH (2016) Pathogenic mechanism of recurrent mutations of SCN8A in epileptic encephalopathy. Ann Clin Transl Neurol 3:114–123. CrossRef Medline

Witter MP, Groenewegen HJ, Lopes da Silva FH, Lohman AH (1989) Functional organization of the extrinsic and intrinsic circuitry of the parahippocampal region. Prog Neurobiol 33:161–253. CrossRef Medline

Yamada-Hanff J, Bean BP (2013) Persistent sodium current drives conditional pacemaking in CA1 pyramidal neurons under muscarinic stimulation. J Neurosci 33:15011–15021. CrossRef Medline

Yue C, Remy S, Su H, Beck H, Yaari Y (2005) Proximal persistent Na+ channels drive spike after depolarizations and associated bursting in adult CA1 pyramidal cells. J Neurosci 25:9704–9720. CrossRef Medline